p-Type PbSe and PbS Quantum Dot Solids Prepared with Short-Chain Acids and Diacids

Mohammad H. Zarghami, Yao Liu, Markelle Gibbs, Eminet Gebremichael, Christopher Webster, and Matt Law*

Department of Chemistry, Department of Chemical Engineering and Materials Science, University of California, Irvine, Irvine, California 92697

ABSTRACT We show that ligand exchange with short-chain carboxylic acids (formic, acetic, and oxalic acid) can quantitatively remove oleic acid from the surface of PbSe and PbS quantum dot (QD) films to yield p-type, carboxylate-capped QD solids with field-effect hole mobilities in the range of 10^{-4}—10^{-1} cm^2 V^{-1} s^{-1}. For a given chemical treatment, PbSe devices have 10-fold higher mobilities than PbS devices because of stronger electronic coupling among the PbSe QDs and possibly a lower density of surface traps. Long-term optical and electrical measurements (i) show that carboxylate-capped PbSe QD films oxidize much more gradually in air than do thiol-capped PbSe films and (ii) quantify the slower and less extensive oxidation of PbS relative to PbSe QDs. We find that whereas the hole mobility of thiol-capped samples decreases continuously with time in air, the mobility of carboxylate-capped films first increases by an order of magnitude over several days before slowly decreasing over weeks. This behavior is a consequence of the more robust binding of carboxylate ligands to the QD surface, such that adsorbed oxygen and water initially boost the hole mobility by passivating surface states and only slowly degrade the ligand passivation to establish an oxide shell around each QD in the film. The superior hole mobilities and oxidation resistance of formic- and acetic-treated QD solids may prove useful in constructing efficient, stable QD photovoltaic devices.

KEYWORDS: quantum dots · PbSe · PbS · field-effect transistors · solar cells

Solar cells with active layers consisting of pure films of colloidal semiconductor quantum dots (QDs) are objects of growing scientific and technological interest.[1−3] Thin film QD photovoltaics can be made using large-area, low-cost solution methods such as roll-to-roll coating, and may provide a pathway to ultrahigh conversion efficiencies via multiple exciton generation (MEG).[4,5] Films of electronically coupled QDs (often called QD solids) also represent a versatile new class of granular conductors with which to investigate electronic confinement, multicarrier physics,[6,7] doping, and junction formation in nanoscale systems. These materials retain the optoelectronic properties of their constitutive QDs if gentle techniques are used to couple the QDs together without destroying them. Thin film QD solar cells are thus distinct from solar cells made from sintered (bulk-like) layers of solution-deposited nanocrystals, an approach now demonstrated with colloidal CdTe/CdSe,[8] CuInSe$_2$ and related compounds,[9−11] and Cu$_2$ZnSnS$_4$.[12−14] Cost reduction, rather than efficiency enhancement, is the main motivation for fabricating sintered polycrystalline active layers from nanocrystal inks or paints.

QD photovoltaic devices based on thin films of PbS,[15−17] PbSe,[18−21] PbSe$_x$S$_{1-x}$,[22] and Cu$_2$S[23] colloids have been demonstrated. These devices are typically prepared by dip coating or spin coating a layer of QDs on a substrate and then replacing the original long-chain, insulating organic ligands with a short-chain molecule to decrease the inter-QD spacing and create a conductive QD film.[24−26] Lead salt QDs are the primary focus of research because they combine the principal features needed for facile charge transport in QD assemblies (i.e., high densi-

ties of states, large exciton radii and dielectric constants, and excellent size monodispersity) with strong light absorption and optimal bandgap ranges for MEG[27] (0.5−1.1 eV). The first thin film QD solar cells utilized an ITO/QD/metal Schottky geometry.[15,18] Although Schottky-type cells suffer from low voltages, this device structure remains an important platform for studying MEG because large QDs with MEG-relevant bandgaps can be employed in the active layer. More recently, superstrate heterojunction QD cells utilizing ZnO window layers[21] or underlayers[20] have been reported. The window layer design offers important efficiency advantages, including a shallow charge-separating junction (which allows for a thicker active layer without quantum efficiency falloff at the blue end of the spectrum) and a larger built-in voltage. State-of-the-art QD cells now achieve

(uncertified) power conversion efficiencies of 3−4%.[20]

Most of the lead salt QD cells reported to date use either 1,2-ethanedithiol (EDT) or 1,4-benzenedithiol (BDT) for ligand exchange, but these two molecules are not particularly well suited to making efficient, stable solar cells. First, adsorbed EDT and BDT are susceptible to oxidation by molecular oxygen, and the resulting loss of ligand passivation triggers film oxidation and device degradation.[25] EDT is known to quench MEG in PbSe QD films,[7] while BDT-treated PbSe films have low carrier mobilities (typically $10^{-4}−10^{-3}$ cm^2 V^{-1} s^{-1}),[19] perhaps in part because BDT is a relatively long ligand (S−S distance of ∼6.4 Å). Furthermore, thiol-treated Pb-chalcogenide QD films suffer from short carrier diffusion lengths (typically ∼100 nm)[15,18,28] that limit the external quantum efficiency at longer wavelengths and thus the overall device efficiency. A larger toolbox of short-chain ligands capable of producing robust, MEG-active QD films with long carrier diffusion lengths would help to accelerate the development of high-performance QD photovoltaics.

Here we investigate the impact of short-chain carboxylic acids (formic, acetic, and oxalic acid) on the structural and electronic properties of PbSe and PbS QD solids. We show that these treatments quickly and quantitatively remove oleic acid from films of 6-nm diameter PbSe QDs to yield p-type, carboxylate-capped QD solids with hole mobilities as high as 4×10^{-2} cm^2 V^{-1} s^{-1} (before air exposure) when measured in a field-effect transistor (FET) geometry. Acid-treated PbSe QD films are much more resistant to oxidation than thiol-treated films. In particular, whereas EDT-treated FETs (initially ambipolar) become highly hole doped and ungateable after seconds in air, acid-treated films behave as p-FETs with hole mobilities that increase gradually over several days in air before slowly decreasing over the course of weeks.

Formic, acetic, and oxalic acid treatments are also used to prepare carboxylate-capped films of 8.8-nm diameter PbS QDs. Longer treatment times are required to remove oleate from PbS QDs, and the hole mobilities of the resulting FETs are 10 times lower than for the equivalent PbSe QD devices (maximum of 2×10^{-3} cm^2 V^{-1} s^{-1} before air exposure). Upon air exposure, EDT-treated PbS films rapidly convert from ambipolar to p-type conduction, but the subsequent decline in hole mobility with storage in air is much slower than for EDT-treated PbSe FETs. In air, the hole mobilities of the acid-treated PbS FETs increase by an order of magnitude (to as high as 2×10^{-2} cm^2 V^{-1} s^{-1}, 10−30 times larger than the mobility of EDT-treated films) before peaking and slowly decreasing in a manner similar to the air-exposed PbSe FETs. Our data support a two-stage oxidation process in which adsorption of oxygen and water first increases the hole mobility by passivating surface states and subsequently decreases the mobility by establishing an oxide shell around each QD in the film. By combining respectable hole mobilities with improved surface passivation and oxidation resistance, these acid treatments may prove useful in enhancing the performance of Schottky and heterojunction QD solar cells.

RESULTS AND DISCUSSION

Acid-Treated PbSe QD Films. To elucidate the impact of formic, acetic, and oxalic acid treatments on PbSe QD solids, we first prepared a series of ∼400-nm thick QD films by spin coating a 300 mg mL^{-1} solution of 6.1-nm diameter, oleate-capped PbSe QDs in octane onto silicon substrates. Untreated (as-made) QD films were compared with films treated in solutions of the various acids by Fourier transform infrared (FTIR) spectroscopy in order to monitor the ligand exchange process and quantify the displacement of oleate (Figure 1). Presumably this ligand exchange occurs by protonation of oleate by the free short-chain acids, resulting in desorption of oleic acid and adsorption, to varying degrees, of oxalate, formate, or acetate. Oxalic acid is the most aggressive treatment: soaking spin-cast films in 1 mM oxalic acid in acetonitrile for 1 min removes essentially all (>98%) of the original oleate from the surface of the QDs, as determined from integrated C−H stretch intensities in the FTIR spectra, and adds a substantial amount of oxalate to the film, signaled by the appearance of strong ν_{as}(COO) and ν_s(COO) vibrations at 1612 and 1294 cm^{-1}.[29,30] The absence of carbonyl stretching at ∼1700 cm^{-1} and hydroxyl signal above 3000 cm^{-1} suggests that the oxalate ligands are completely deprotonated. This, combined with the moderate frequency difference between the antisymmetric and symmetric carboxylate absorption bands ($\Delta\nu_{as-s} = 318$ cm^{-1}), indicates that the adsorbed oxalate probably adopts a chelating and/or bidentate bridging geometry either as an anion on a single QD or as a linker between two QDs (Scheme S1 in the Supporting Information).[31] Scanning electron microscopy (SEM) images of oxalate-treated films show marked QD clustering consistent with oxalate linkages between QDs (Figure 2). Similar clumping is also observed in films treated in 10 mM formic acid solutions, while 2 mM formic acid treatments yield homogeneous, unclumped films, as does acetic acid (Figure 2). FTIR, optical absorption, X-ray diffraction, and FET mobility measurements collectively rule out any etching of the QDs as well as the presence of an organic or inorganic matrix in the oxalate- and formate-capped films. We speculate that the clumped appearance of these films results from a combination of QD−QD binding (in the case of oxalate) and strong QD−QD attraction induced by complete removal of oleate and the very short carboxylate ligands.

Although oxalic acid is a fairly strong acid in water (pK_{a1} = 1.3) and might etch QDs treated in this solvent, it is a much weaker acid in acetonitrile (pK_a = 14.5)[32] and both optical absorption and X-ray diffraction (XRD) measurements of oxalic-treated films show
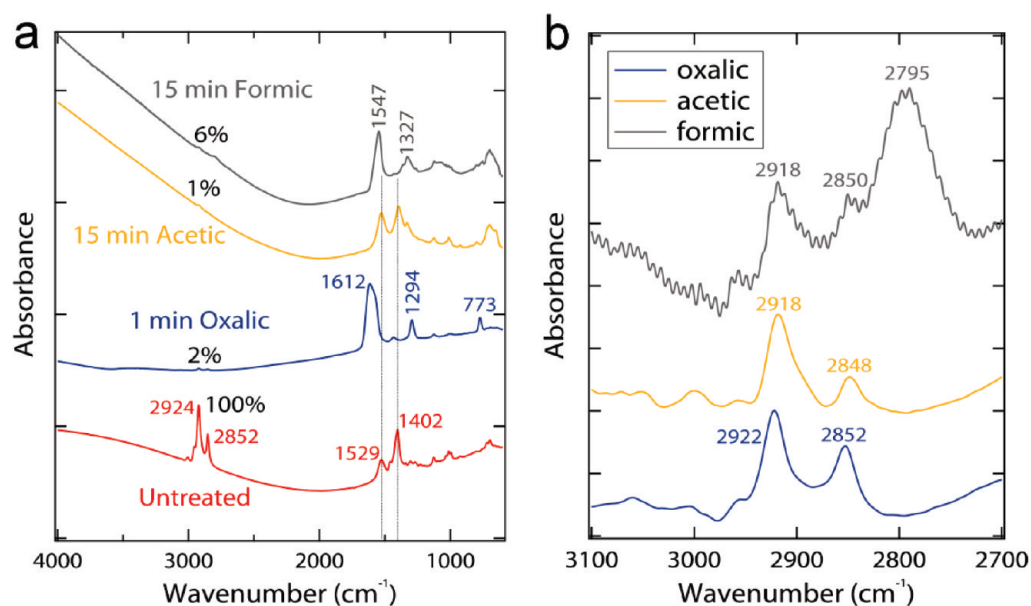
Figure 1. FTIR spectra of films of 6.1 nm PbSe QDs made by spin-casting onto silicon substrates and treated in 1 mM oxalic, 10 mM acetic, or 10 mM formic acid solutions in acetonitrile: (a) survey scans for three films and an untreated oleate-capped control film; (b) magnification of the C−H stretching region of the treated films. All films were 400 nm-thick before treatment. The sloping backgrounds are caused by optical interference effects (see Figures S1−S3 in the Supporting Information for additional spectra).

that no QD etching occurs. Absorption spectra of oxalate-coated films on glass substrates show a 14 meV redshift of the first excitonic peak upon exchange of oleate with oxalate (Figure 3); etching would result in a blueshift of ∼75 meV for even a 5 Å decrease in QD diameter. This redshift, which is similar in magnitude to redshifts observed after treating PbSe QD solids in formic or acetic acid (Figure 3), hydrazine,[26] or dithiols,[25] arises from a combination of increased average dielectric constant and enhanced inter-QD electronic coupling when oleate is removed and the QDs pack closer together within a film.[25] Any redshift of the excitonic energy due to decreased electronic confinement from the ligand exchange itself—often observed when ole-

ate is replaced with amines or thiols—is probably insignificant here because oleate is replaced by other carboxylates, leaving the molecular environment at the QD surface largely unaltered. XRD measurements confirm that the QD size is unchanged (to within ±1 Å) by exposure to 1 mM oxalic acid, even for soaking times as long as 20 min (the longest studied) (Supporting Information, Figure S4). On the basis of such optical and XRD data, we conclude that each of the three acid treatments replaces oleate without etching the QDs, unsurprising given the small dissociation constants of these carboxylic acids in acetonitrile.

Formic acid and acetic acid treatments require higher concentrations and longer immersion times to
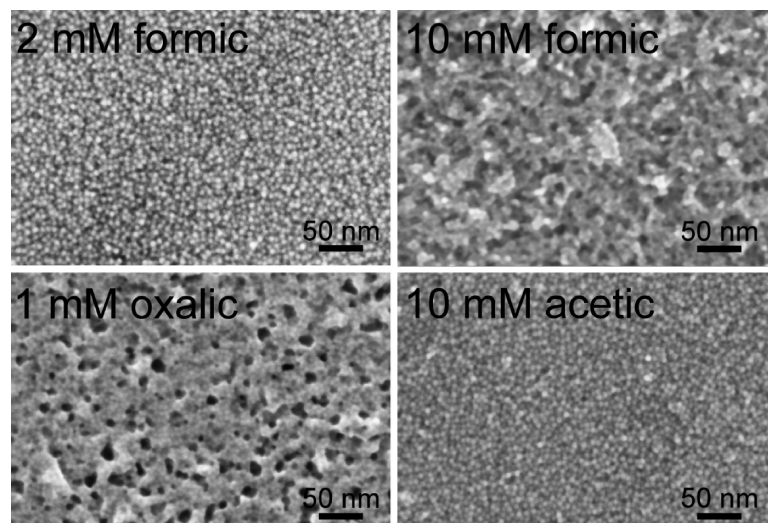

Figure 2. SEM images of ∼100-nm thick films of 6.1 nm carboxylate-capped PbSe QDs prepared by dip coating on silicon substrates (see Supporting Information Figure S5 for an image of an untreated film prepared by spin coating).
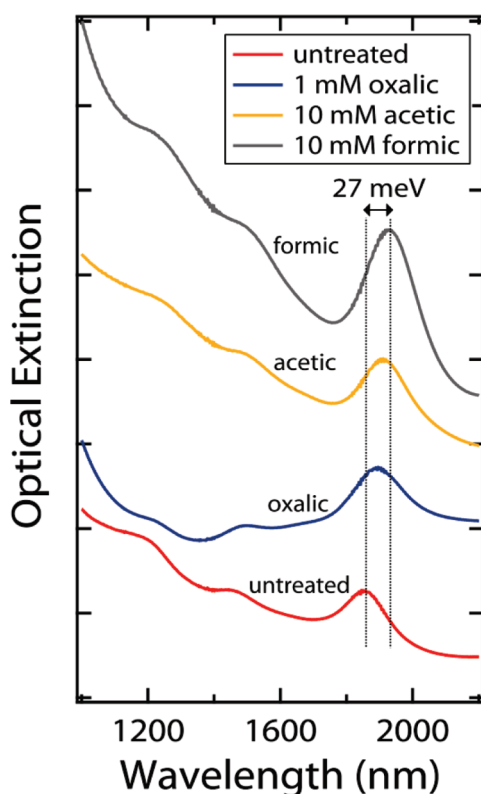
Figure 3. Optical absorption spectra of carboxylate-capped PbSe QD films (6.2 nm QDs) prepared by dip coating on glass substrates. The untreated film was prepared by spin coating. Measurements were performed in an air-free sample cell in transmission mode. The first exciton absorption of the untreated film occurs at 1857 nm (E_g = 0.668 eV).

completely remove of oleate from spin-cast QD films but are otherwise similar to the oxalate exchange. Formic-treated samples show FTIR peaks at 1547 and 1327 cm^{-1} that are consistent with the ν_{as}(COO) and
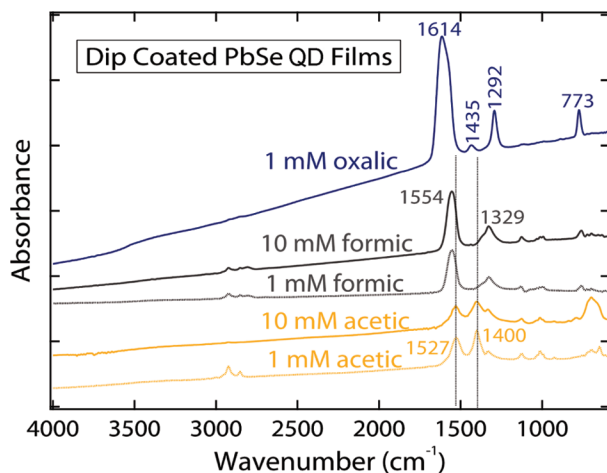

Figure 4. FTIR spectra of carboxylate-capped films of 6.1 nm PbSe QDs made by layer-by-layer dip coating on silicon substrates. Identical dip coating parameters were used for all films (50 cycles at a dipping speed of 0.35 m per minute and 3−5 s immersion times), with the exception that a rinsing step was added in the case of oxalic acid treatments to prevent the accumulation of (nonvolatile) oxalic acid in the growing films. Note that untreated films cannot be made by this dip-coating process, which is why spin-cast films are used to quantify oleate removal.

ν_s(COO) vibrations of chemisorbed formate.[33] Magnification of the C−H stretching region (Figure 1b) reveals the presence of adsorbed formate (ν(CH) or ν_s(COO) + δ(CH) modes at 2795 cm^{-1})[34−36] along with a small amount of residual oleate (peaks at 2918 and 2850 cm^{-1}, present after all three acid treatments). The feature at 2795 cm^{-1} occurs only in the films treated with formic acid. Meanwhile, acetic-treated samples lose nearly all C−H stretch intensity and show minimal shifts in the frequencies of their carboxylate bands relative to the oleate-coated control films. The reason for the absence of C−H intensity expected from the methyl group of adsorbed acetate is currently unclear. Values of $\Delta\nu_{as-s}$ for formic- and acetic-treated films (220 and 127 cm^{-1}, respectively) support a chelating and/or bidentate bridging geometry of the two carboxylate ions on the QD surface, as observed previously on metal oxide nanocrystals.[35]

Spin-cast QD films are useful for assessing the results of the acid treatments but suffer from serious disadvantages in optoelectronic applications, including batch-to-batch irreproducibility, nonuniformity over large areas, and cracking due to volume loss upon ligand exchange. To avoid these problems, we used layer-by-layer dip coating to prepare uniform, crack-free acid-treated QD films. In this dip-coating process, QD solids are grown in a stepwise fashion by repeatedly immersing substrates in a solution of QDs and then a treatment solution that removes oleate, thereby insolubilizing each newly added layer of QDs to gradually build up a conductive film. FTIR spectra show that dip coating with acid treatments of sufficient concentration (1−10 mM) results in quantitative removal of oleate along with some degree of adsorption of the short-chain acids (Figure 4). Peak positions and relative intensities are in good agreement with the results from the spin-cast films (Figure 1). We have noticed in the course of these experiments that the fraction of oleate removed can be controlled by changing the concentration of the acid solution and the immersion time per dipping cycle, which suggests a route to the fabrication of graded films with tunable doping, carrier mobility, and conductivity.

Acid-Treated PbS QD Films. FTIR results from spin-cast films of 8.8-nm diameter PbS QDs are presented in Figure 5. The acid treatments have the same general effect as with the PbSe QDs but require longer immersion times to achieve the same degree of oleate removal. The slower action of the treatments may reflect stronger binding of oleate to PbS. Films prepared by dip coating show qualitatively similar FTIR and optical absorption spectra to the spin-cast PbS samples and to the PbSe films (Figure 6). There are some minor differences in the ν_{as}(COO) and ν_s(COO) vibrational frequencies between the acid-coated PbS and PbSe films. Oxalic acid and acetic acid are again the most aggressive and least aggressive treatments, respectively. Whereas 1
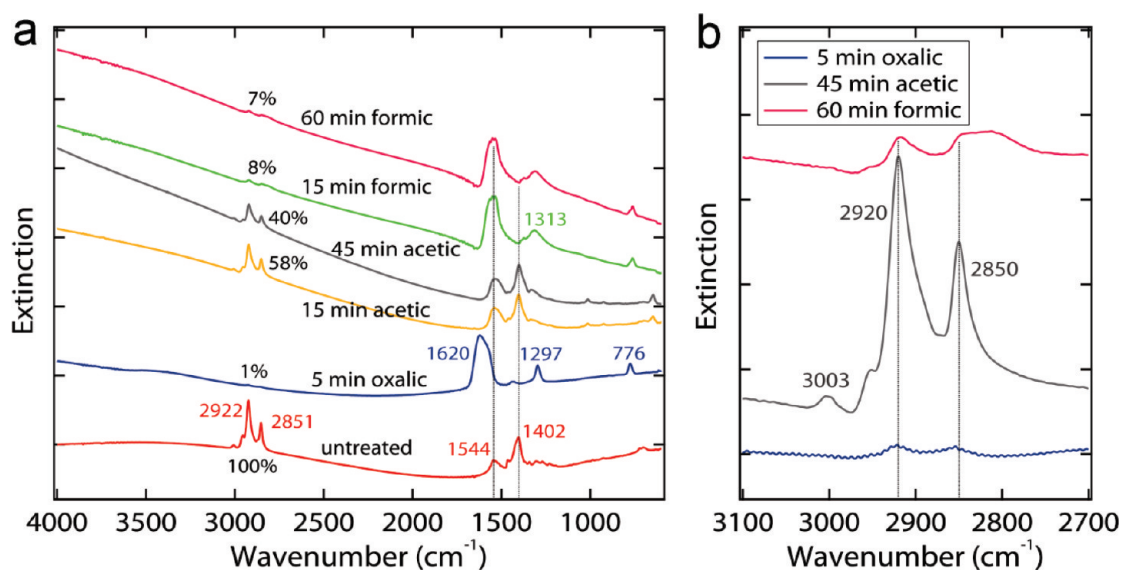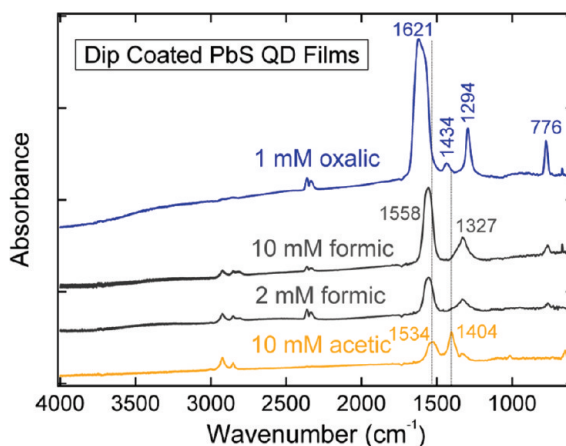
Figure 5. FTIR spectra of films of 8.8 nm PbS QDs made by spin-casting onto silicon substrates and treated in 1 mM oxalic, 10 mM acetic, or 10 mM formic acid solutions in acetonitrile: (a) survey scans. (b) magnification of the C−H stretching region of the treated films. All films were 350 nm-thick before treatment (see Figure S6 in the Supporting Information for structural characterization of these PbS QDs).

mM oxalic acid removes ∼100% of the original oleate after 5 min, 10 mM acetic acid treatments remove only ∼60% of the C−H stretching signal from spin-cast films even after 45 min, implying that substantial oleate remains in the acetic-treated PbS films. The dip-coated PbS films with the most residual oleate are also acetic acid treated (Figure 6). Residual oleate is expected to result in a large inter-QD spacing, poor electronic coupling, and particularly low carrier mobilities for acetic-treated PbS QD FETs. Despite this prediction, we find that mobility values increase in the order oxalic < acetic < formic for both PbS and PbSe QD films (see below). This trend shows that the degree of removal of the long-chain ligand does not by itself determine the carrier mobility in QD films. This may be because greater oleate removal fails to correlate with decreased inter-QD distance and/or increased strength of inter-QD electronic coupling. Other factors, such as the surface trap state density, which depends strongly on surface chemistry, also influence mobility. Figure 7 presents optical absorption spectra of the acid-treated PbS films. While acetic- and formic-treated samples show the typical redshift relative to the untreated controls, oxalate-capped films sometimes have blueshifted excitonic transitions. The blueshift is sample dependent: we observe a blueshift in ∼50% of the oxalic-treated samples and a small redshift in the other 50%. XRD rules out etching of the QDs by oxalic acid as the cause of the blueshift. We propose, consistent with the low mobilities of oxalate-capped films, that oxalate-treated QD solids are weakly coupled and that the blueshift, when it occurs, reflects an enhanced degree of electronic confinement in oxalate-coated QDs relative to oleate-coated QDs, the precise origin of which is unclear.

Electrical Measurements. We measured the electrical conductivity and carrier mobility of the acid-treated PbSe and PbS QD solids in a field-effect transistor (FET) geometry. QD films 20−30 nm thick were dip coated onto oxidized silicon substrates prepatterned with gold source and drain electrodes. The current flowing between these two electrodes (I_D) in response to an applied bias (V_{SD}) was modulated by the application of a separate bias to the underlying silicon wafer (V_G), and the slopes of the resulting $I_D−V_G$ plots were used to calculate the carrier mobility of each film in the linear regime, μ_{lin}. All measurements were performed in a glovebox in the dark and at room temperature. Representative current−voltage curves of formic-treated PbSe and PbS QD FETs are shown in Figure 8, and our results are compiled in Table 1. All of the acid-treated QD films act as *p*-type depletion mode FETs

Figure 6. FTIR spectra of carboxylate-capped films of 8.8 nm PbS QDs made by layer-by-layer dip coating on silicon substrates. Film thicknesses are as follows: oxalic = 120 nm, 10 mM formic = 80 nm, 2 mM formic = 40 nm, acetic = 60 nm.
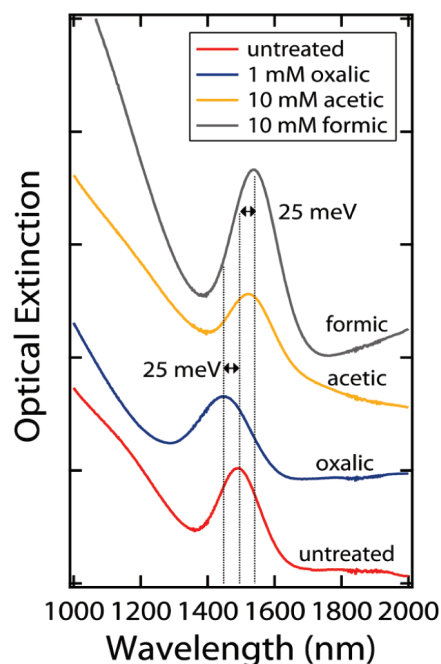
Figure 7. Optical absorption spectra of carboxylate-capped PbS QD films (8.8 nm QDs) prepared by dip coating on glass substrates. The untreated film was prepared by spin coating. Measurements were performed in an air-free sample cell in transmission mode. The first exciton absorption of the untreated film occurs at 1490 nm (E_g = 0.832 eV).

with hole currents that cannot be turned off. Formic-treated PbSe QD FETs show the highest currents and

mobilities (μ_{lin} = $2-4 \times 10^{-2}$ cm^2 V^{-1} s^{-1}), while oxalic-treated PbSe devices have mobilities about 10 times smaller (2×10^{-3} cm^2 V^{-1} s^{-1}) and acetic-treated devices are in between ($6-7 \times 10^{-3}$ cm^2 V^{-1} s^{-1}). Hole mobilities of the PbS FETs follow the same trend but are 10−20 times lower than their PbSe counterparts (*e.g.*, $1-2 \times 10^{-4}$ cm^2 V^{-1} s^{-1} for oxalic-treated PbS devices). The larger physical diameter and smaller exciton Bohr radius of the PbS QDs results in weaker electronic coupling and therefore lower mobilities for the PbS FETs. It is also possible that a larger density of active surface traps contributes to the smaller carrier mobility of the PbS films.

We observe quasi-linear $I_{SD}-V_D$ curves without saturation of I_{SD} (*i.e.*, no pinch-off), suggesting large hole densities in the FET channel (or, equivalently, a large positive threshold voltage, V_T, such that $V_D > V_G - V_T$). Conductivities of the PbSe FETs are fairly high, ranging between 5×10^{-4} S cm^{-1} (oxalic acid) to 10^{-2} S cm^{-1} (formic acid). Thus, although the mobility of formic-treated PbSe films is nearly the same as that of EDT-treated PbSe films for the same QD size,[37] formic treatments result in 50−100 fold larger conductivities and carrier densities relative to EDT treatments. Such a high conductivity and hole concentration may limit the ability of carboxylate-capped QD active layers to generate large voltages in solar cells. On the other hand, the PbS
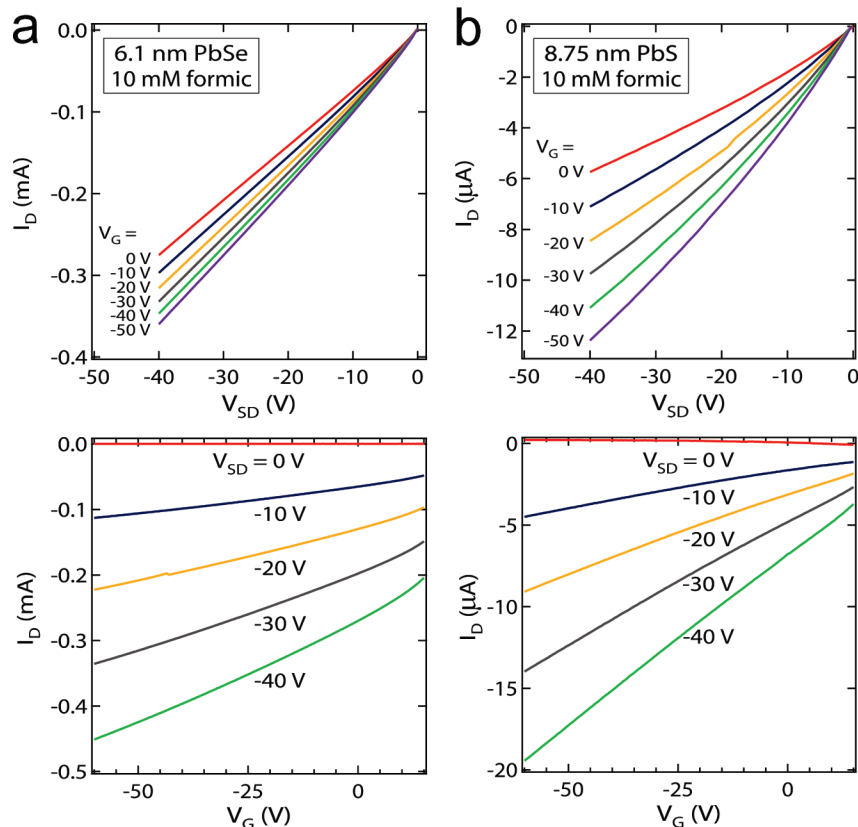

Figure 8. Electrical characteristics of PbSe and PbS QD FETs. Output and transfer curves of (a) a 10 mM formic-treated PbSe QD film (6.1 nm QDs) and (b) a 10 mM formic-treated PbS QD film (8.8 nm QDs). Channel dimensions: length = 10 μm; width = 1000 μm; film thickness = 20−30 nm (see Supporting Information Figures S7 and S8 for data from the other films).

TABLE 1. Electronic Properties of Acid-Treated PbSe and PbS QD FETs

QD	treatment	type	mobility (cm^2 V^{-1} s^{-1})	conductivity^a (S cm^{-1})	hole density^b (cm^{-3})
6.1 nm PbSe	10 mM formic	p	$(3.7 \pm 0.1) \times 10^{-2}$	1.0×10^{-2}	2×10^{18}
	10 mM acetic	p	$(6.9 \pm 1.6) \times 10^{-3}$	6.2×10^{-4}	6×10^{17}
	1 mM oxalic	p	$(2.3 \pm 1.5) \times 10^{-3}$	5.3×10^{-4}	2×10^{18}
6.0 nm PbSe	10 mM formic	p	$(2.3 \pm 0.4) \times 10^{-2}$	4.3×10^{-2}	1×10^{19}
	2 mM formic	p	$(1.1 \pm 0.1) \times 10^{-2}$	6.0×10^{-3}	3×10^{18}
	10 mM acetic	p	$(6.0 \pm 0.3) \times 10^{-3}$	2.3×10^{-3}	2×10^{18}
	1 mM oxalic	p	$(2.5 \pm 0.2) \times 10^{-3}$	1.0×10^{-3}	3×10^{18}
8.8 nm PbS	10 mM formic	p	$(2.4 \pm 0.7) \times 10^{-3}$	7.6×10^{-4}	2×10^{18}
	2 mM formic	p	$(1.6 \pm 0.6) \times 10^{-3}$	3.0×10^{-4}	1×10^{18}
	10 mM acetic	p	$(3.8 \pm 0.5) \times 10^{-4}$	1.1×10^{-4}	2×10^{18}
	1 mM oxalic	p	$(1.5 \pm 0.4) \times 10^{-4}$	3.2×10^{-5}	1×10^{18}

^{a}Zero-field conductivity is calculated at $V_G = 0$ V, ignoring contact resistances, known to be less than 10% of the film resistance. ^{b}Calculated from $\sigma = pe\mu$ at $V_G = 0$ V. Note that a random close-packed array of 6-nm diameter QDs contains 6×10^{18} QDs per cubic centimeter, while a similar array of 8.75-nm diameter QDs contains 2×10^{18} QDs cm^{-3}.

films have fairly low conductivities ranging from 3×10^{-5} S cm^{-1} (oxalic acid) to 8×10^{-4} S cm^{-1} (formic acid), which should lead to lower dark currents and better voltage generation in solar cells. It is interesting to note that the *effective* hole density, $p = \sigma/(e\mu)$, is a fairly constant quantity for all of the devices, averaging 2×10^{18} cm^{-3}, which translates to ~1 hole for every 3 PbSe QDs or 1 hole per PbS QD for our films.

Oxidation Studies. QD films are susceptible to oxidation at ambient conditions because they have large internal surface areas and high surface energies.[38] Surface oxidation often results in drastic changes in the electronic properties of PbSe QD films, most typically a large increase in conductivity induced by hole doping and ligand desorption upon short-term exposure to air. Hydrazine- and alkanethiol-treated PbSe films are particularly unstable,[25,26] whereas PbS QD films are generally more resistant to oxidation, presumably because sulfide is a poorer reducing agent than the other chalcogenides.[39] Oxidative degradation remains a major obstacle to the long-term stability of solar cells built from lead salt QDs.[19,40] We hypothesized that small carboxylate ligands would confer enhanced oxidation resistance to PbSe and PbS QD films compared to the thiol ligands now in widespread use in QD devices because they can bind strongly to surface Pb atoms, pack densely, and resist oxidative desorption. Oxalic acid should be particularly effective since it is nonvolatile and capable of chelating the QD surface, possibly even linking QDs together into a dense 3D covalent organic–inorganic solid.

We studied the oxidation of acid-treated PbSe and PbS QD films by monitoring the energy of the first excitonic peak in absorption spectra acquired as a function of time in laboratory air and light. Blueshifts of the excitonic energy reflect an increased degree of quantum confinement as the surface of the QDs oxidizes and the QD cores become progressively smaller, both physically and electronically. Figures 9 and 10 plot the excitonic energy for oxalic-, formic-, and acetic-treated

films during the first month of storage in air. The films generally show an initial rapid blueshift over the course of minutes to days followed by an asymptotic stabilization of the excitonic energy after days to weeks. This trend is consistent with a two-stage oxidation process in which rapid adsorption of oxygen/water and partial ligand hydrolysis are followed by the slow growth of a thin, self-saturating oxide shell (mostly PbO, PbOH$_2$, and
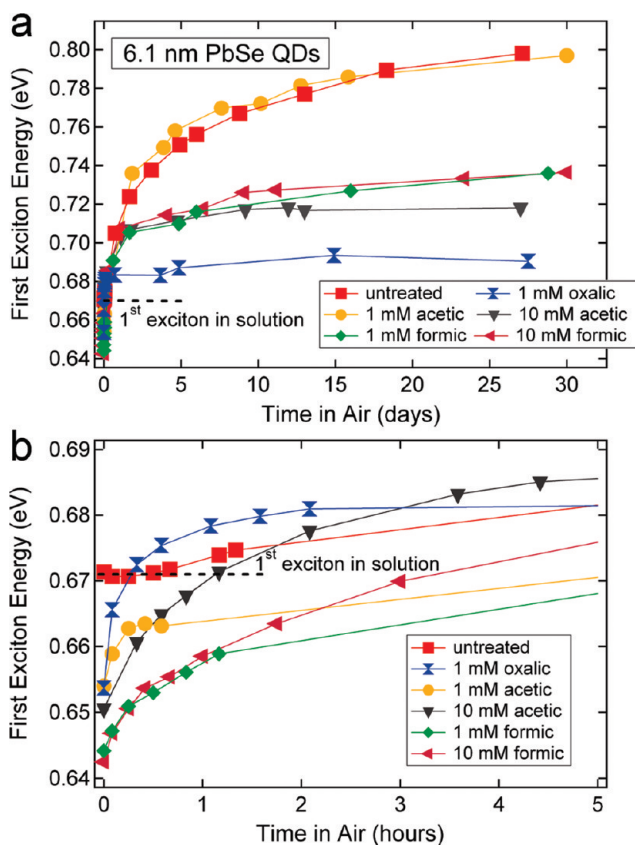

Figure 9. Energy of the first excitonic transition as a function of time in air for acid-treated, dip-coated PbSe QD films on glass substrates: (a) time traces out to one month of air exposure; (b) time traces for the first 5 h of air exposure. The untreated control film was prepared by spin coating. Dotted lines indicate the exciton energy for solutions of the QDs in tetrachloroethylene (see Supporting Information, Figure S9 for the original spectra of these samples).
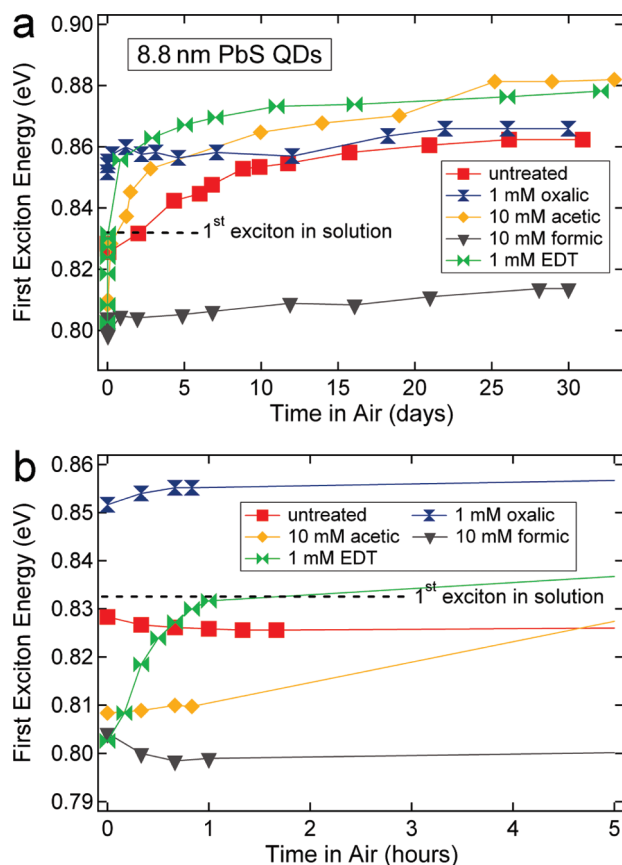
Figure 10. Energy of the first excitonic transition as a function of time in air for acid- and EDT-treated, dip-coated PbS QD films on glass substrates: (a) time traces out to one month of air exposure; (b) time traces for the first 5 h of air exposure. The untreated control film was prepared by spin coating. Dotted lines indicate the exciton energy of the QDs in solution.

PbSeO$_3$)[25] around each QD in the film. We note that the untreated films and the formic-treated PbS films actually *redshift* slightly (1−5 meV) over the first few minutes to hours before eventually blueshifting. The cause of this transitory redshift is unclear, but it may indicate a competition during the early stages of oxidation of some films between factors that decrease QD electronic confinement/isolation (*i.e.*, a narrowing of the surface bandgap or increase in the dielectric constant due to water/oxygen diffusion into the films and adsorption on the QDs) and factors that enhance QD confinement/isolation (principally the conversion of surface PbSe/PbS into oxides). Further study is required to understand these processes in greater detail.

Although all of the PbSe and PbS QD films oxidize to some extent, the degree of oxidation depends strongly on the type of QD and ligand. PbSe oxidizes more quickly and more extensively than does PbS. The more rapid oxidation of PbSe is evident in the magnified views of the initial hours of air exposure (Figures 9b and 10b); here, the untreated PbSe films blueshift by ~10 meV after 5 h but the untreated PbS films show no blueshift until 24 h after air exposure. After one month, the untreated PbSe films show an overall blue-

shift of ~125 meV, equivalent to approximately a 1 nm decrease in QD core diameter and the growth of a wide-bandgap oxide shell slightly thinner than a single PbSe unit cell (as determined from diameter-bandgap curves of oleate-capped QDs; see Supporting Information Figure S10). In contrast, the blueshift of untreated PbS films over the same period is ~34 meV, equivalent to a reduction of the QD diameter by ~0.5 nm and a oxide wide gap layer about half of a unit cell thick.

Of the acid-treated PbSe films, the oxalate-coated samples are the most robust against oxidation, showing blueshifts of only 37 meV, compared to 94 meV for formic- and 68 meV for acetic-treated samples. This is consistent with the notion that oxalate forms a chelate complex with the QD surface that is particularly resistant to hydrolysis. Note, however, that oxalic-treated PbSe samples show surprisingly pronounced blueshifts at short times in air, suggesting that the oxalate ligands do not effectively shield all regions of the QD surface from chemisorbed oxygen and water. In addition to surface selenium ions, which likely remain unpassivated after the carboxylate ligand exchanges, it is possible that oxalate packs inefficiently and leaves small domains of unpassivated Pb ions that are vulnerable to oxidative attack. Although not shown in Figure 9, we find that EDT- and BDT-treated PbSe films oxidize more rapidly and extensively than any of the acid-treated samples, with overall blueshifts of 150−180 meV after one month in air.

Gauged by their absorption spectra, the most stable QD films we have tested are the formic- and oxalic-treated PbS samples, with overall blueshifts of only 10 and 14 meV, respectively, after one month in air. EDT-treated PbS films, in contrast, show the most rapid and pronounced blueshifting (nearly 80 meV) of any of the PbS films (Figure 10). The dramatic changes we observe with EDT-treated films indicate that EDT quickly desorbs from the QD surface upon exposure to air, leaving behind a bare QD film that is particularly susceptible to oxidation.

We measured the performance of all of the PbSe and PbS FETs as a function of storage time in air; the results are collected in Figure 11. We first discuss the impact of air exposure on EDT-treated PbSe and PbS FETs in order to set a baseline for the other films. Before air exposure, the EDT-capped films behave as ambipolar transistors (both electron and hole transport). Exposing EDT-treated PbSe samples to air for 20 s results in a large increase in conductivity, the loss of n-channel conduction as well as nearly all gate modulation, and a dramatic decrease in hole mobility, consistent with previous results[25] (Figure 11a). EDT-treated PbS films are significantly more robust than EDT-treated PbSe films: upon air exposure, the PbS devices also convert from ambipolar to p-channel behavior, but the hole mobility decreases more slowly, dropping ~20% after 24 h in air (Figure 11a). These observations are consistent with
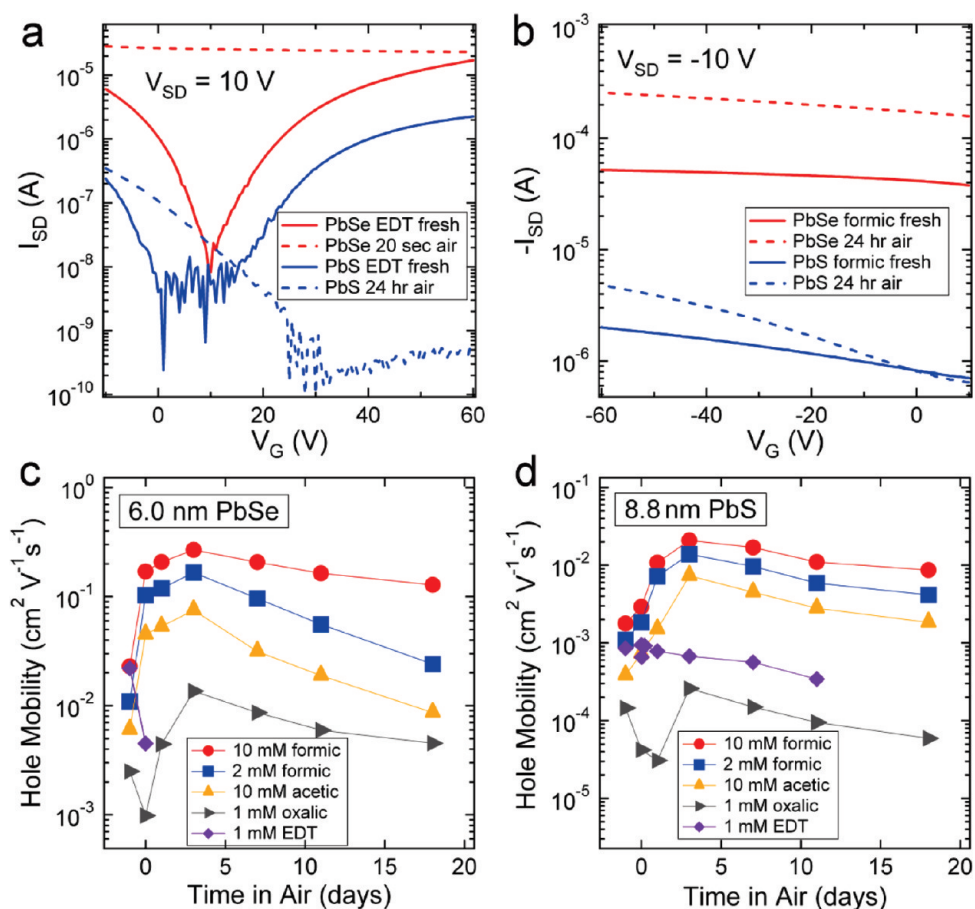
Figure 11. Electrical performance of PbSe and PbS QD FETs as a function of time in air: (a) transfer curves ($I_D - V_G$) of EDT-treated PbSe and PbS FETs before and after air exposure; (b) transfer curves of formic-treated PbSe and PbS FETs; (c) time traces of the hole mobility of carboxylate-capped PbSe FETs with time in air; (d) time traces for PbS FETs. The first and second data points of each trace indicate the mobility before air exposure and after 5 min in air, respectively (see Supporting Information, Figures S11 and S12 for typical current−voltage plots of these devices).

an oxidation mechanism in which the oxidative desorption of EDT (i) produces surface traps, lowering the carrier mobility, and (ii) exposes the film surface to attack by oxygen and water, which dopes the films with holes[41] and further decreases the mobility. We believe that PbS changes more gradually because it binds EDT more strongly and is more resistant to oxidation than PbSe.

The acid-treated FETs show quite different behavior in air. For example, the hole mobility of formic-treated FETs *increases* by about an order of magnitude during the first 24 h of air exposure (Figure 11b). Measured over longer periods of time, the mobility of the acid-treated films is observed to increase by a factor of 10−20 during the first 72 h in air and then gradually decrease over the subsequent weeks (except the oxalic-treated PbS samples, which show only a 2-fold mobility increase) (Figure 11c,d). We attribute the initial increase in mobility to the passivation of surface states by adsorbed oxygen and water and the subsequent decrease in mobility to gradual hydrolysis of the carboxylate ligands and ensuing oxide layer formation. In contrast, the mobility of the EDT-treated FETs decreases monotonically with time in air, rapidly in the case of

PbSe and more gradually for PbS. The essential difference between EDT-capped and carboxylate-capped FETs is apparently the more robust surface passivation provided by the carboxylate ligands. We note that the rate of mobility increase for the acid-capped films is highest for the PbSe devices, again reflecting the more labile PbSe surface. Formic-treated PbSe and PbS devices show the highest peak mobilities of 0.3 and 0.02 cm^2 V^{-1} s^{-1}, an order of magnitude larger than the hole mobilities of pristine EDT-treated films. The larger majority-carrier mobilities of air-exposed formic- and acetic-treated films may prove advantageous in the construction of QD solar cells with improved carrier diffusion lengths.

CONCLUSION

We have shown that ligand exchange with short-chain carboxylic acids can quantitatively remove oleate to yield p-type PbSe and PbS QD films with field-effect hole mobilities in the range of 10^{-4}−10^{-1} cm^2 V^{-1} s^{-1}. The relatively high conductivity of these films suggests that acid capping generates a large free hole concentration ($\sim$10^{18} cm^{-3}). PbS devices show 10-fold

lower mobilities than PbSe devices made using the same film treatment. PbS field-effect transistors prepared with EDT are much more stable in air than EDT-treated PbSe QD films, but the n-channels of both films disappear upon air exposure and the hole mobilities decrease monotonically with time in air (at very different rates). Long-term FET measurements demonstrate that the hole mobilities of acid-treated films exposed to air increase by a factor of 10−20 before gradually decreasing. At the same time, optical absorption spectra of the acid-treated films show a monotonic, treatment-dependent increase in exciton energy and carrier confinement as oxidation unfolds. Our results therefore show that the mobility of QD films can increase despite a concurrent decrease in inter-QD coupling. This can be understood in the case of acid-treated PbSe and PbS FETs if initial oxidation results in the passivation of surface traps and if oxidation of the film surface is relatively slow because the carboxylate ligands are strongly bound. More detailed future studies of the interplay among surface chemistry, oxidation, and the mobility and lifetime of charge carriers in QD films will provide valuable guidance for the fabrication of efficient and truly stable QD photovoltaic devices.

METHODS

Materials. Lead oxide (PbO, 99.999%), selenium (99.99%), oleic acid (OA, tech. grade, 90%), diphenylphosphine (DPP, 98%), 1-octadecene (ODE, 90%), acetic acid (glacial, 99.99%), oxalic acid (anhydrous), and anhydrous solvents were purchased from Aldrich and used as received. Bis(trimethylsilyl) sulfide (TMS) was acquired from Gelest, while trioctylphosphine (TOP, technical grade, > 90%) and 1,2-ethanedithiol (EDT, > 98%) were from Fluka and formic acid (99+%) was from Acros.

QD Synthesis. PbSe QDs were synthesized and purified using standard air-free techniques. In a typical synthesis, 1.09 g PbO (4.9 mmol), 3.45 g OA (12.2 mmol), and 13.25 g ODE were degassed in a three-neck flask for 10 min at room temperature and 10 min at 100 °C, then heated at 180 °C for at least 1 h under flowing nitrogen to dissolve the PbO and dry the solution. Next, 15 mL of a 1 M TOP-Se solution (15 mmol) containing 0.13 mL DPP was rapidly injected into the hot lead oleate solution. PbSe QD nucleation was instantaneous. Once the desired growth time had elapsed (1−20 min), the reaction was quenched with a water bath and the injection of 15 mL of dry hexane. The QDs were purified by precipitation three times in hexane/ethanol and stored in a glovebox.

PbS QDs were prepared using a procedure adapted from Hines.[42] Briefly, 0.65 g PbO (2.9 mmol) and 12.7 g OA (57 mmol) were mixed, degassed as described above, heated at 150 °C for at least 1 h, and cooled to 100 °C before a solution of 0.3 mL TMS (1.4 mmol) in 5.6 g ODE was rapidly injected. The reaction was immediately quenched with a water bath and the QDs were purified similarly to the PbSe QD samples.

Fabrication of QD Films. Both spin coating and dip coating were used to make QD films. Films were spin coated inside of a glovebox from 300 mg mL^{-1} solutions of PbSe or PbS QDs in octane, then immersed in 5 mL of a 1, 2, or 10 mM solution of the appropriate short-chain acid in dry acetonitrile for a given time. Samples treated in oxalic acid were rinsed with dry acetonitrile to remove any oxalic acid residue (oxalic acid is nonvolatile at room temperature).

Films were dip coated using a layer-by-layer procedure described in detail elsewhere[25,28] with a mechanical dip coater mounted inside of a glovebox (DC Multi-4, Nima Technology). The substrates (prepatterned FET substrates, glass slides, or double-side-polished i-Si(100) wafers, cleaned by sonication in acetone followed by rinses in acetone and hexane and drying under an N$_2$ flow) were repetitively dipped into a 2 mg mL^{-1} solution of QDs in dry hexane and then a 1, 2, or 10 mM solution of the appropriate short-chain acid in dry acetonitrile. In the case of the oxalic acid treatments, a third beaker containing pure acetonitrile was used to rinse the films after each dip in the oxalic acid solution. We fabricated films with thicknesses in the range of 20−450 nm (thin for FETs and thick for UV−vis and FTIR studies).

Characterization. Transmission electron microscopy (TEM) characterization was performed on a Philips CM 20 operating at 200 kV. A Zeiss Ultra 55 Plus field emission scanning electron microscope (SEM) was used to image the QD films. Optical absorption data were acquired with a PerkinElmer Lambda 950 spectrophotometer equipped with an integrating sphere. Fourier transform infrared (FTIR) data were taken with a Jasco 4100 FTIR spectrometer. A Rigaku Ultima III diffractometer was used for X-ray diffraction measurements.

Field-Effect Transistor Measurements. QD films were dip cast onto degenerately doped silicon substrates that were coated with a 200-nm-thick thermal SiO$_2$ gate oxide and patterned with source/drain electrodes (5 nm Ti/35 nm Au; 5, 10, or 25 μm channel length, 1000 μm width). Film thicknesses of 20−35 nm (3−6 QD diameters) were used. Unwanted areas of each film were removed with a swab. FET measurements were performed in a glovebox with a homemade probe station using a Keithley 2636A dual-channel SourceMeter driven by LabVIEW software. Consistent with previous results[26,36] we found the source-drain currents of these FETs to be time dependent (quasi-exponential decay) upon a change in gate voltage. I_D-V_{SD} and I_D-V_G curves were therefore acquired as quickly as possible (0.4−0.8 s) to minimize the distorting effects of the slow transient process(es) on the output and transfer characteristics of the devices. Electron and hole mobilities μ_{lin} were calculated from transfer curves acquired at positive and negative V_{SD}, respectively, according to the gradual channel approximation equation in the linear regime,

$$\frac{\partial I_D}{\partial V_G}\bigg|_{V_{SD}=constant} = \frac{WC_{ox}V_{SD}}{L}\mu_{lin}$$

where W is the channel width, L the channel length, and C_{ox} is the capacitance per unit area of the gate oxide. The carrier mobilities reported here are averages of 3−6 devices.

Supporting Information Available: Additional figures and schemes. This material is available free of charge *via* the Internet at http://pubs.acs.org.

REFERENCES AND NOTES

1. Nozik, A. J. Quantum Dot Solar Cells. *Phys. E* **2002**, *14*, 115−120.
2. Hillhouse, H. W.; Beard, M. C. Solar Cells from Colloidal Nanocrystals: Fundamentals, Materials, Devices, and Economics. *Curr. Opin. Colloid Interface Sci.* **2009**, *14*, 245−259.
3. Sargent, E. H. Infrared Photovoltaics Made by Solution Processing. *Nat. Photonics* **2009**, *3*, 325−331.

4. Schaller, R. D.; Klimov, V. I. High Efficiency Carrier Multiplication in PbSe Nanocrystals: Implications for Solar Energy Conversion. *Phys. Rev. Lett.* **2004**, *92*, 186601.

5. Ellingson, R. J.; Beard, M. C.; Johnson, J. C.; Yu, P. R.; Micic, O. I.; Nozik, A. J.; Shabaev, A.; Efros, A. L. Highly Efficient Multiple Exciton Generation in Colloidal PbSe and PbS Quantum Dots. *Nano Lett.* **2005**, *5*, 865–871.

6. Luther, J. M.; Beard, M. C.; Song, Q.; Law, M.; Ellingson, R. J.; Nozik, A. J. Multiple Exciton Generation in Films of Electronically Coupled PbSe Quantum Dots. *Nano Lett.* **2007**, *7*, 1779–1784.

7. Beard, M. C.; Midgett, A. G.; Law, M.; Semonin, O. E.; Ellingson, R. J.; Nozik, A. J. Variations in the Quantum Efficiency of Multiple Exciton Generation for a Series of Chemically-Treated PbSe Nanocrystal Films. *Nano Lett.* **2009**, *9*, 836–845.

8. Gur, I.; Fromer, N. A.; Geier, M. L.; Alivisatos, A. P. All-Inorganic Nanocrystal Solar Cells Processed from Solution. *Science* **2005**, *310*, 462–465.

9. Guo, Q.; Kim, S. J.; Kar, M.; Shafarman, W. N.; Birkmire, R. W.; Stach, E. A.; Agrawal, R.; Hillhouse, H. W. Development of CuInSe$_2$ Nanocrystal and Nanoring Inks for Low-Cost Solar Cells. *Nano Lett.* **2008**, *8*, 2982–2987.

10. Guo, Q.; Ford, G. M.; Hillhouse, H. W.; Agrawal, R. Sulfide Nanocrystal Inks for Dense Cu(In$_{1-x}$Ga$_{3x}$)(S$_{1-3y}$Se$_y$)$_2$ Absorber Films and Their Photovoltaic Performance. *Nano Lett.* **2009**, *9*, 3060–3065.

11. Panthani, M. G.; Akhavan, V.; Goodfellow, B.; Schmidtke, J. P.; Dunn, L.; Dodabalapur, A.; Barbara, P. F.; Korgel, B. A. Synthesis of CuInS$_2$, CuInSe$_2$, and Cu(In$_x$Ga$_{1-x}$)Se$_2$ (CIGS) Nanocrystal "Inks" for Printable Photovoltaics. *J. Am. Chem. Soc.* **2008**, *130*, 16770–16771.

12. Guo, Q; Hillhouse, H. W.; Agrawal, R. Synthesis of Cu$_2$ZnSnS$_4$ Nanocrystal Ink and Its Use for Solar Cells. *J. Am. Chem. Soc.* **2009**, *131*, 11672–11673.

13. Steinhagen, C.; Panthani, M. G.; Akhavan, V.; Goodfellow, B.; Koo, B.; Korgel, B. A. Synthesis of Cu$_2$ZnSnS$_4$ Nanocrystals for Use in Low-Cost Photovoltaics. *J. Am. Chem. Soc.* **2009**, *131*, 12554–12555.

14. Riha, S. C.; Parkinson, B. A.; Prieto, A. L. Solution-Based Synthesis and Characterization of Cu$_2$ZnSnS$_4$ Nanocrystals. *J. Am. Chem. Soc.* **2009**, *131*, 12054–12055.

15. Johnston, K. W.; Pattantyus-Abraham, A. G.; Clifford, J. P.; Myrskog, S. H.; MacNeil, D. D.; Levina, L.; Sargent, E. H. Schottky-Quantum Dot Photovoltaics for Efficient Infrared Power Conversion. *Appl. Phys. Lett.* **2008**, *92*, 151115.

16. Tsang, S. W.; Fu, H.; Wang, R.; Lu, J.; Yu, K.; Tao, Y. Highly Efficient Cross-Linked PbS Nanocrystal/C60 Hybrid Heterojunction Photovoltaic Cells. *Appl. Phys. Lett.* **2009**, *95*, 183505.

17. Sun, B.; Findikoglu, A. T.; Sykora, M.; Werder, D. J.; Klimov, V. I. Hybrid Photovoltaics Based on Semiconductor Nanocrystals and Amorphous Silicon. *Nano Lett.* **2009**, *9*, 1235–1241.

18. Luther, J. M.; Law, M.; Song, Q.; Reese, M. O.; Beard, M. C.; Ellingson, R. J.; Nozik, A. J. Schottky Solar Cells Based on Colloidal Nanocrystal Films. *Nano Lett.* **2008**, *8*, 3488–3492.

19. Koleilat, G. I.; Levina, L.; Shukla, H.; Myrskog, S. H.; Hinds, S.; Pattantyus-Abraham, A.; Sargent, E. H. Efficient, Stable Infrared Photovoltaics Based on Solution-Cast Colloidal Quantum Dots. *ACS Nano* **2008**, *2*, 833–840.

20. Choi, J. J.; Lim, Y.-F.; Santiago-Berrios, M. B.; Oh, M.; Hyun, B. R.; Sun, L.; Bartnik, A. C.; Goedhart, A.; Malliaras, G. G.; Abruña, H. D.; Wise, F. W.; Hanrath, T. PbSe Nanocrystal Excitonic Solar Cells. *Nano Lett.* **2009**, *9*, 3749–3755.

21. Leschkies, K. S.; Beatty, T. J.; Kang, M. S.; Norris, D. J.; Aydil, E. S. Solar Cells Based on Junctions between Colloidal PbSe Nanocrystals and Thin ZnO Films. *ACS Nano* **2009**, *3*, 3638–3648.

22. Ma, W.; Luther, J. M.; Zheng, H. M.; Wu, Y.; Alivisatos, A. P. Photovoltaic Devices Employing Ternary PbS$_x$Se$_{1-x}$ Nanocrystals. *Nano Lett.* **2009**, *9*, 1699–1703.

23. Wu, Y.; Wadia, C.; Ma, W.; Sadtler, B.; Alivisatos, A. P. Synthesis and Photovoltaic Application of Copper(I) Sulfide Nanocrystals. *Nano Lett.* **2008**, *8*, 2551–2555.

24. Talapin, D. V.; Murray, C. B. PbSe Nanocrystal Solids for n- and p-Channel Thin Film Field-Effect Transistors. *Science* **2005**, *310*, 86–89.

25. Luther, J. M.; Law, M.; Song, Q.; Beard, M. C.; Nozik, A. J. Structural, Optical, and Electrical Properties of Self-Assembled Films of PbSe Nanocrystals Treated with 1,2-Ethanedithiol. *ACS Nano* **2008**, *2*, 271–280.

26. Law, M.; Luther, J. M.; Song, Q.; Hughes, B. K.; Perkins, C. L.; Nozik, A. J. Structural, Optical, and Electrical Properties of PbSe Nanocrystal Solids Treated Thermally or with Simple Amines. *J. Am. Chem. Soc.* **2008**, *130*, 5974–5985.

27. Hanna, M. C.; Nozik, A. J. Solar Conversion Efficiency of Photovoltaic and Photoelectrolysis Cells with Carrier Multiplication Absorbers. *J. Appl. Phys.* **2006**, *100*, 074510.

28. Law, M.; Beard, M. C.; Choi, S.; Luther, J. M.; Hanna, M. C.; Nozik, A. J. Determining the Internal Quantum Efficiency of PbSe Nanocrystal Solar Cells with the Aid of an Optical Model. *Nano Lett.* **2008**, *8*, 3904–3910.

29. Pettibone, J. M.; Cwiertny, D. M.; Scherer, M.; Grassian, V. H. Adsorption of Organic Acids on TiO$_2$ Nanoparticles: Effects of pH, Nanoparticle Size, and Nanoparticle Aggregation. *Langmuir* **2008**, *24*, 6659–6667.

30. Dobson, K. D.; McQuillan, A. J. *In situ* Infrared Spectroscopic Analysis of the Adsorption of Aliphatic Carboxylic Acids to TiO$_2$, ZrO$_2$, Al$_2$O$_3$, and Ta$_2$O$_5$ from aqueous solutions. *Spectrochim. Acta, Part A* **1999**, *55*, 1395–1405.

31. Alcock, N. W.; Tracy, V. M.; Waddington, T. C. Acetates and Acetato-Complexes. Part 2. Spectroscopic Studies. *J. Chem. Soc., Dalton* **1976**, 2243–2246.

32. Eckert, F.; Leito, I.; Kaljurand, I.; Kütt, A.; Klamt, A.; Diedenhofen, M. Prediction of acidity in acetonitrile solution with COSMO-RS. *J. Comput. Chem.* **2009**, *30*, 799–810.

33. Rotzinger, F. P.; Kesselman-Truttmann, J. M.; Hug, S. J.; Shklover, V.; Gratzel, M. Structure and Vibrational Spectrum of Formate and Acetate Adsorbed from Aqueous Solution onto the TiO$_2$ Rutile (110) Surface. *J. Phys. Chem. B* **2004**, *108*, 5004–5017.

34. Millar, G. J.; Rochester, C. H.; Waugh, K. C. An FTIR Study of the Adsorption of Formic Acid and Formaldehyde on Potassium-Promoted Cu/SiO$_2$ Catalysts. *J. Catal.* **1995**, *155*, 52–58.

35. Calatayud, M.; Collins, S. E.; Baltanás, M. A.; Bonivardi, A. L. Stability of Formate Species on α-Ga$_2$O$_3$. *Phys. Chem. Chem. Phys.* **2009**, *9*, 1397–1405.

36. Chen, M.-T.; Lin, Y.-S.; Lin, Y.-F.; Lin, H.-P.; Lin, J.-L. Dissociative Adsorption of HCOOH, CH$_3$OH, and CH$_2$O on MCM-41. *J. Catal.* **2004**, *228*, 259–263.

37. Liu, Y.; Gibbs, M.; Puthussery, J.; Ihly, R.; Law, M. Manuscript in press.

38. van Huis, M. A.; Kunneman, L. T.; Overgaag, K.; Xu, Q.; Pandraud, G.; Zandbergen, H. W.; Vanmaekelbergh, D. Low-Temperature Nanocrystal Unification through Rotations and Relaxations Probed by *in Situ* Transmission Electron Microscopy. *Nano Lett.* **2008**, *8*, 3959–3963.

39. Klem, E. J. D.; Shukla, H.; Hinds, S.; MacNeil, D. D.; Levina, L.; Sargent, E. H. Impact of Dithiol Treatment and Air Annealing on the Conductivity, Mobility, and Hole Density in PbS Colloidal Quantum Dot Solids. *Appl. Phys. Lett.* **2008**, *92*, 212105.

40. Tang, J.; Wang, X.; Brzozowski, L.; Barkhouse, D. A. R.; Debnath, R.; Levina, L.; Sargent, E. H. Schottky Quantum Dot Solar Cells Stable in Air under Solar Illumination. *Adv. Mater.* **2010**, *22*, 1–5.

41. Rogacheva, E. I.; Tavrina, T. V.; Nashchekina, O. N.; Grigorov, S. N.; Sipatov, A. Y.; Volobuev, V. V.; Dresselhaus, M. S.; Dresselhaus, G. Influence of Oxidation on the Transport Properties of IV−VI Thin Films. *Phys. E* **2003**, *17*, 310–312.

42. Hines, M. A.; Scholes, G. D. Colloidal PbS Nanocrystals with Size-Tunable Near-Infrared Emission: Observation of Post-Synthesis Self-Narrowing of the Particle Size Distribution. *Adv. Mater.* **2003**, *15*, 1844–1849.